PLASMA FLOWS IN THE HELIOSHEATH ALONG THE VOYAGER 1 AND 2 TRAJECTORIES DUE TO EFFECTS OF THE 11 YR SOLAR CYCLE

The Astrophysical Journal, 794:29 (9pp), 2014 October 10 doi:10.1088/0004-637X/794/1/29

PLASMA FLOWS IN THE HELIOSHEATH ALONG THE *VOYAGER 1* AND *2* TRAJECTORIES DUE TO EFFECTS OF THE 11 YR SOLAR CYCLE

E. Provornikova[1,2,3], M. Opher[4], V. V. Izmodenov[3,5,6], J. D. Richardson[7], and G. Toth[8]
[1] Department of Physics, Catholic University of America, Washington, DC 20064, USA; elena.a.provornikova@nasa.gov
[2] NASA Goddard Space Flight Center, Code 671, Greenbelt, MD 20771, USA
[3] Space Research Institute of RAS, Moscow, 117997, Russia
[4] Astronomy Department, Boston University, Boston, MA 02215, USA; mopher@bu.edu
[5] Lomonosov Moscow State University, Moscow, 119991, Russia; izmod@iki.rssi.ru
[6] Institute for Problems in Mechanics, Moscow, 119526, Russia
[7] Kavli Center for Astrophysics and Space Research, Massachusetts Institute of Technology, Cambridge, MA 02139, USA; jdr@space.mit.edu
[8] University of Michigan, Ann Arbor, MI 48109, USA; gtoth@umich.edu
Received 2013 July 1; accepted 2014 July 26; published 2014 September 22

ABSTRACT

We investigate the role of the 11 yr solar cycle variations in the solar wind (SW) parameters on the flows in the heliosheath using a new three-dimensional time-dependent model of the interaction between the SW and the interstellar medium. For boundary conditions in the model we use realistic time and the latitudinal dependence of the SW parameters obtained from *SOHO*/SWAN and interplanetary scintillation data for the last two solar cycles (1990–2011). This data set generally agrees with the in situ *Ulysses* measurements from 1991 to 2009. For the first ∼30 AU of the heliosheath the time-dependent model predicts constant radial flow speeds at *Voyager 2* (*V2*), which is consistent with observations and different from the steady models that show a radial speed decrease of 30%. The model shows that *V2* was immersed in SW with speeds of 500–550 km s^{-1} upstream of the termination shock before 2009 and in wind with upstream speeds of 450–500 km s^{-1} after 2009. The model also predicts that the radial velocity along the *Voyager 1* (*V1*) trajectory is constant across the heliosheath, contrary to observations. This difference in observations implies that additional effects may be responsible for the different flows at *V1* and *V2*. The model predicts meridional flows (VN) higher than those observed because of the strong bluntness of the heliosphere shape in the N direction in the model. The modeled tangential velocity component (VT) at *V2* is smaller than observed. Both VN and VT essentially depend on the shape of the heliopause.

Key words: interplanetary medium – magnetohydrodynamics (MHD) – solar wind – Sun: activity – Sun: heliosphere

Online-only material: color figures

1. INTRODUCTION

Since crossing the termination shock (TS), *Voyager 1* (*V1*) and *Voyager 2* (*V2*) have experienced very different plasma flows in the heliosheath. The plasma instrument is not working on *V1* and flow speeds are determined from LECP data using the Compton-Getting effect (Decker et al. 2005). Immediately after crossing the TS, *V2* experienced an average radial speed of 130 km s^{-1}. At the end of 2009, the radial speed dropped to about 100 km s^{-1} and since then has remained essentially constant with an average speed of 110 km s^{-1}. The non-radial velocity components at *V2* increased as the flow turned around the heliopause (HP) toward the heliotail (Richardson et al. 2009; Richardson & Wang 2012). The radial speed at *V1* after the TS was about 80 km s^{-1}, which is lower than the actual for *V2* after crossing the TS, and this has decreased almost linearly across the heliosheath. Steady-state models of the outer heliosphere do not explain the constant radial speed maintained by *V2* and the gradual decrease of the radial speed to zero for *V1* within 30 AU inside the heliosheath.

Several models demonstrated that effects of the solar cycle strongly influence the TS and HP locations and flows in the heliosheath (Karmesin et al. 1995; Wang & Belcher 1999; Baranov & Zaitsev 1998; Zank 1999; Scherer & Fahr 2003; Zank & Muller 2003; Izmodenov et al. 2005, 2008; Pogorelov et al. 2009). In a three-dimensional time-dependent model, Washimi et al. (2011) used *V2* data during 2001–2008 for boundary conditions, assuming that the solar wind (SW) parameters vary by a factor of 1.5 from slow to fast SW, and they reproduced the *V1* and *V2* TS crossings. Pogorelov et al. (2012) modeled an idealized solar cycle and showed that regions with negative radial velocity formed near the HP. Using a model with boundary conditions constructed from *Ulysses* data, Pogorelov et al. (2013) analyzed the TS asymmetry and time variations of the flows and magnetic field in the heliosheath. Boundary conditions in these three-dimensional models are based on in situ measurements along the spacecraft trajectory, e.g., one point in space at a given time. A complete time-dependent model of the outer heliosphere requires realistic three-dimensional time-varying boundary conditions for the SW. The SW parameters should be specified at a given distance from the Sun as functions of heliolatitude, heliolongitude, and time. The main difficulty is that a three-dimensional SW structure cannot be measured in situ. However, time and latitudinal variations of the SW parameters can be derived from indirect observations such as remote radio observations of interplanetary scintillations (IPS; Sokol et al. 2012; Tokumaru et al. 2012) and measured intensities of the backscattered solar Lyα emission (Quemerais et al. 2006; Lallement et al. 2010). Recently, Katushkina et al. (2013) used these data sets to derive the charge exchange hydrogen ionization rates in their model of interstellar hydrogen distribution in the heliosphere. Kubiak et al. (2014) used

SW data from Sokol et al. (2012) to calculate helium ionization rates due to charge exchange with SW protons in their model of helium distribution in the heliosphere (although for helium, this charge exchange ionization rate is three orders smaller than photoionization).

In this paper, we demonstrate the effects of a realistic solar cycle on the plasma flows in the heliosheath based on results of a three-dimensional MHD model of the outer heliosphere that includes time and latitudinally dependent boundary conditions for the SW during two full solar cycles. We incorporate realistic variations of the SW density and velocity derived from IPS measurements and solar Lyα emission data. This paper focuses on the first 30 AU of the heliosheath where the plasma beta $\beta = p_{\rm th}/p_B > 1$.

2. MODEL AND BOUNDARY CONDITIONS

For this study, we developed a three-dimensional time-dependent MHD multi-fluid model of SW interaction with the local interstellar medium (LISM). The model includes interstellar hydrogen atoms interacting with plasma protons in a charge exchange process. Hydrogen atoms are described in a four-fluid approximation (Opher et al. 2009). The model is based on the BATS-R-US code (Toth et al. 2012). The grid is Cartesian with a Sun-centered spherical inner boundary at 30 AU and an outer boundary of $x = \pm 1000$ AU, $y = \pm 1000$ AU, $z = \pm 1000$ AU box. We use a non-uniform numerical grid with a highly resolved region along the *V2* trajectory with a grid cell size of 0.25 AU (Provornikova et al. 2013) in order to compare model results with direct plasma measurements on *V2*.

Since the dynamic pressure is dominant in the supersonic SW, variations of the plasma density and velocity are most important for the global dynamics of the heliosphere and its boundaries. Recently Sokol et al. (2012) retrieved the heliolatitudinal structure of the SW speed at 1 AU and its evolution in time based on IPS data and the in situ, in ecliptic measurements from the OMNI database. They produced one-year average latitudinal profiles of the SW speed with a resolution of 10° for the two last solar cycles between 1990 and 2011.

Analysis of *SOHO*/SWAN Lyα intensity maps provided the time and heliolatitudinal distribution of the interstellar hydrogen ionization rate at 1 AU for the period 1996–2011 (Quemerais et al. 2006; Lallement et al. 2010). Hydrogen ionization is mainly due to a charge exchange with plasma protons and, to a lesser extent, photoionization. These two components can be separated as described in Katushkina et al. (2013) to obtain the charge exchange rate. The charge exchange rate is a product of the SW mass flux $\rho_{\rm sw} V_{\rm sw}$ and the charge exchange cross-section. The SW density as a function of time and latitude can be calculated from the charge exchange rate by using the IPS-derived SW speed. For this calculation, values of the charge exchange rate averaged over one Carrington rotation (CR) in time and 10° in latitude were used. (To cover the period 1990–1996, the hydrogen ionization rate was assumed to repeat with an 11 yr period.) Thus, the combination of IPS, SWAN, and OMNI (in the ecliptic plane) data gives the heliolatitudinal and time variations of the SW number density $n_{\rm sw}(t, \theta)$ and velocity $V_{\rm sw}(t, \theta)$ at 1 AU from 1990 to 2011 with a resolution of 10°in latitude ($-90° < \theta < 90°$) and one CR in time (the resolution in time for the SW speed data was increased from one year to one CR by linear interpolation).

We compared the SW parameters extracted from the given data set along the *Ulysses* trajectory with the actual *Ulysses* measurements normalized to 1 AU during the years 1991–2009. The comparison of the SW density, velocity, and dynamic pressure is shown in Figure 1. From the top plot, it can be seen that the SW speed derived from IPS data agrees well with the *Ulysses* measurements, as reported by Sokol et al. (2012). In our data set, the SW density was calculated from the SW mass flux obtained from SWAN data using IPS-derived SW speeds. The comparison of the SW density (middle plot in Figure 1) shows that large-scale variations of the SW density used for our boundary conditions agree well with *Ulysses* measurements, although there are differences between these data sets for short periods of time (~1 yr). The SW dynamic pressures are generally in good agreement (bottom plot in Figure 1). The

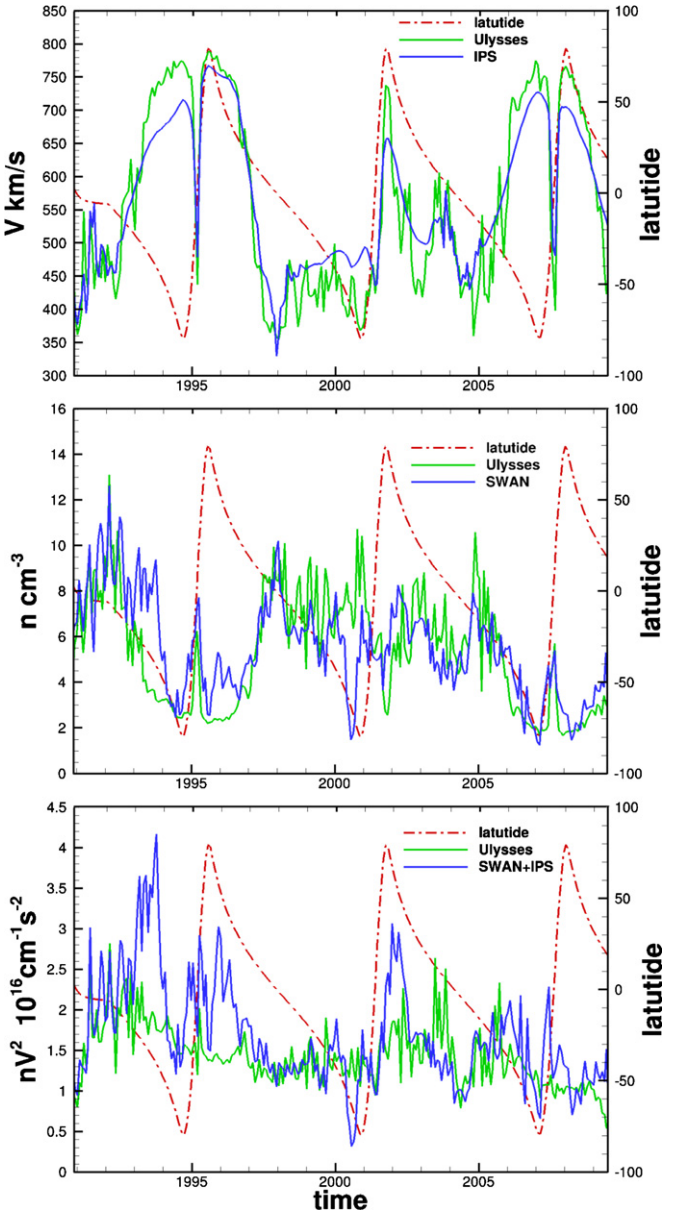

Figure 1. Comparison of the SW parameters extracted along the *Ulysses* trajectory from our SW data set at 1 AU (blue curve) with *Ulysses* in situ measurements (green curve). Top: solar wind speed. Middle: number density. Bottom: dynamic pressure. The red dashed-dot curve shows the *Ulysses* heliolatitude. (Note that the *SOHO*/SWAN data are available only after 1996. The solar wind density for the period 1991–1996 in our data set was calculated from the hydrogen ionization rate extrapolated from SWAN data with an 11 yr period.)

(A color version of this figure is available in the online journal.)

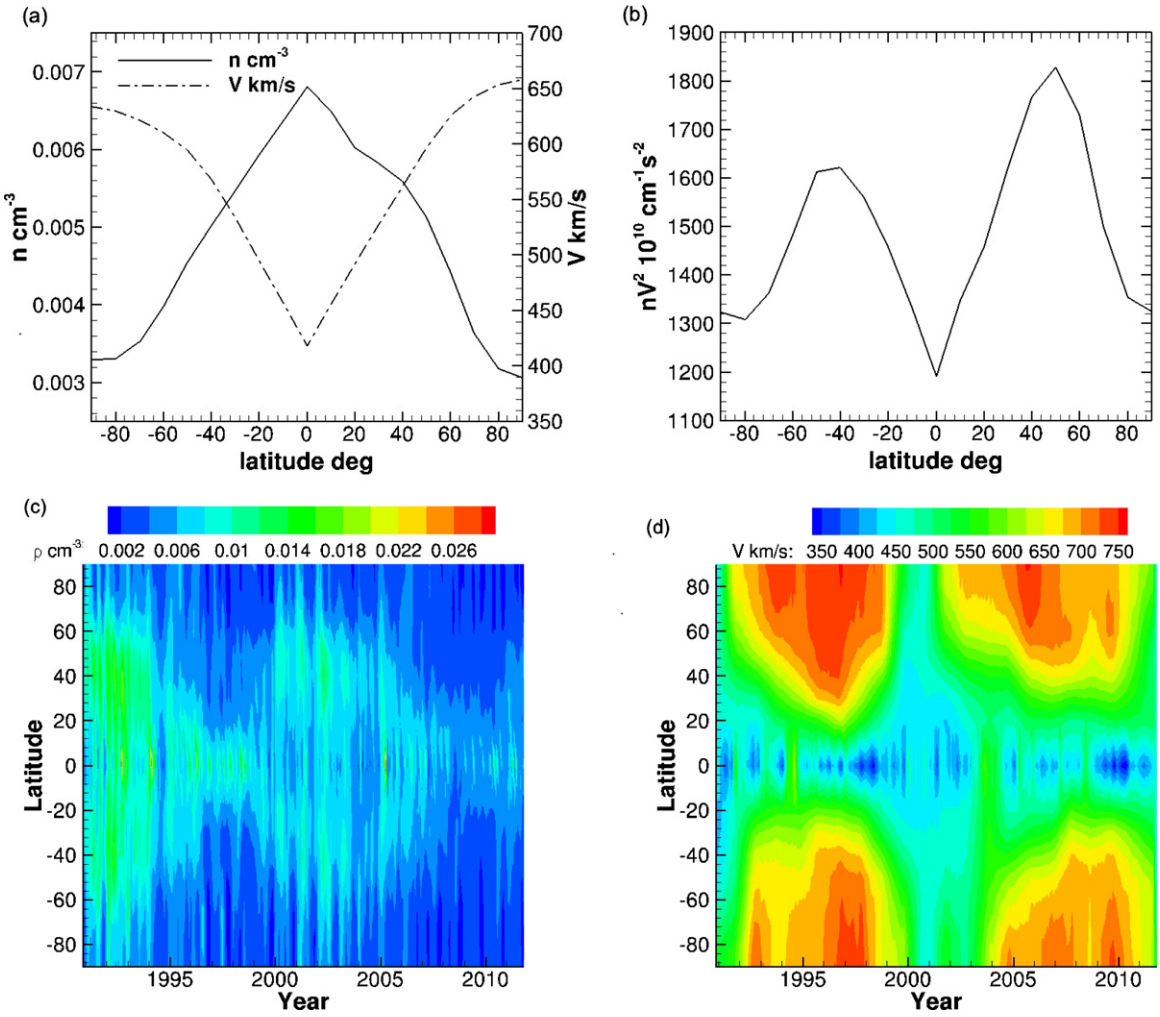

Figure 2. Top panels: (a) boundary conditions for the SW number density and velocity at 30 AU and (b) calculated variations of the dynamic pressure for the three-dimensional steady-state solution. Bottom panels: time-dependent inner boundary conditions at 30 AU for (c) SW number density (cm^{-3}) and (d) velocity (km s^{-1}).

(A color version of this figure is available in the online journal.)

differences in the dynamic pressure are caused mainly by the difference in SW density. *SOHO*/SWAN and *Ulysses* perform essentially different observations: *Ulysses* measures the SW parameters in situ along its trajectory and SWAN measures Lyα intensities which give a longitudinally averaged hydrogen ionization rate. The SW characteristics derived from the SWAN data are therefore expected to differ from locally measured *Ulysses* observations. In general, agreement between *Ulysses* data and our data set is fairly good. We think the SWAN and IPS data capture variations of the SW in time for all latitudes fairly well and thus are suitable to use as input for the study of time-dependent effects in the outer heliosphere.

To obtain time and latitudinal variations of the SW parameters at 30 AU (the inner boundary of the three-dimensional model) we apply a one-dimensional spherically symmetric model of the SW expansion with a highly resolved spatial grid in the radial direction (0.01 AU) for 19 latitudinal directions. This approach does not take into account deflection of the SW flow and the effects of corotating interaction regions (CIRs). CIRs are not resolved in the CR-averaged boundary conditions used at 1 AU. Thus, using a three-dimensional model of the SW starting from 1 AU instead of a one-dimensional model will still not describe CIR effects correctly with this data set and would be more computationally costly. The one-dimensional model includes the effects of interstellar hydrogen atoms (we assumed $n_{H,TS} = 0.08\,\mathrm{cm}^{-3}$, $V_{H,TS} = 24\,\mathrm{km\ s}^{-1}$ at the TS) and takes into account charge exchange and photoionization processes. We use the same one-dimensional model as in Zubkov (2005) but neglect the anomalous cosmic rays component. For each latitudinal direction θ_i ($i = 1, \ldots 19$) we apply the following procedure. First we achieve a steady state solution for the supersonic SW outflow assuming a plasma density n_0, speed V_0 and thermal pressure p_0 for boundary conditions at 1 AU. n_0 and V_0 are obtained from average values of fluxes of mass $n_{\mathrm{sw}}(t, \theta_i)V_{\mathrm{sw}}(t, \theta_i)$ and momentum $n_{\mathrm{sw}}(t, \theta_i)V_{\mathrm{sw}}^2(t, \theta_i)$ at 1 AU over the time period 1990–2011. The thermal pressure p_0 is assumed to be constant for all latitudes at 1 AU and is calculated assuming a Mach number $M = 6$ at the equator, $\theta_i = 0^\circ$. Then, using this steady state, we run a simulation at each latitude θ_i with a time-varying SW density and speed at 1 AU during 1990–2011. Completing the one-dimensional simulation for each direction θ_i, we obtain time and latitudinal variations of the SW plasma parameters at 30 AU for the period 1990–2011. Figures 2(c) and (d) show the SW density and velocity as a function of latitude and time at 30 AU, which are the boundary conditions for our

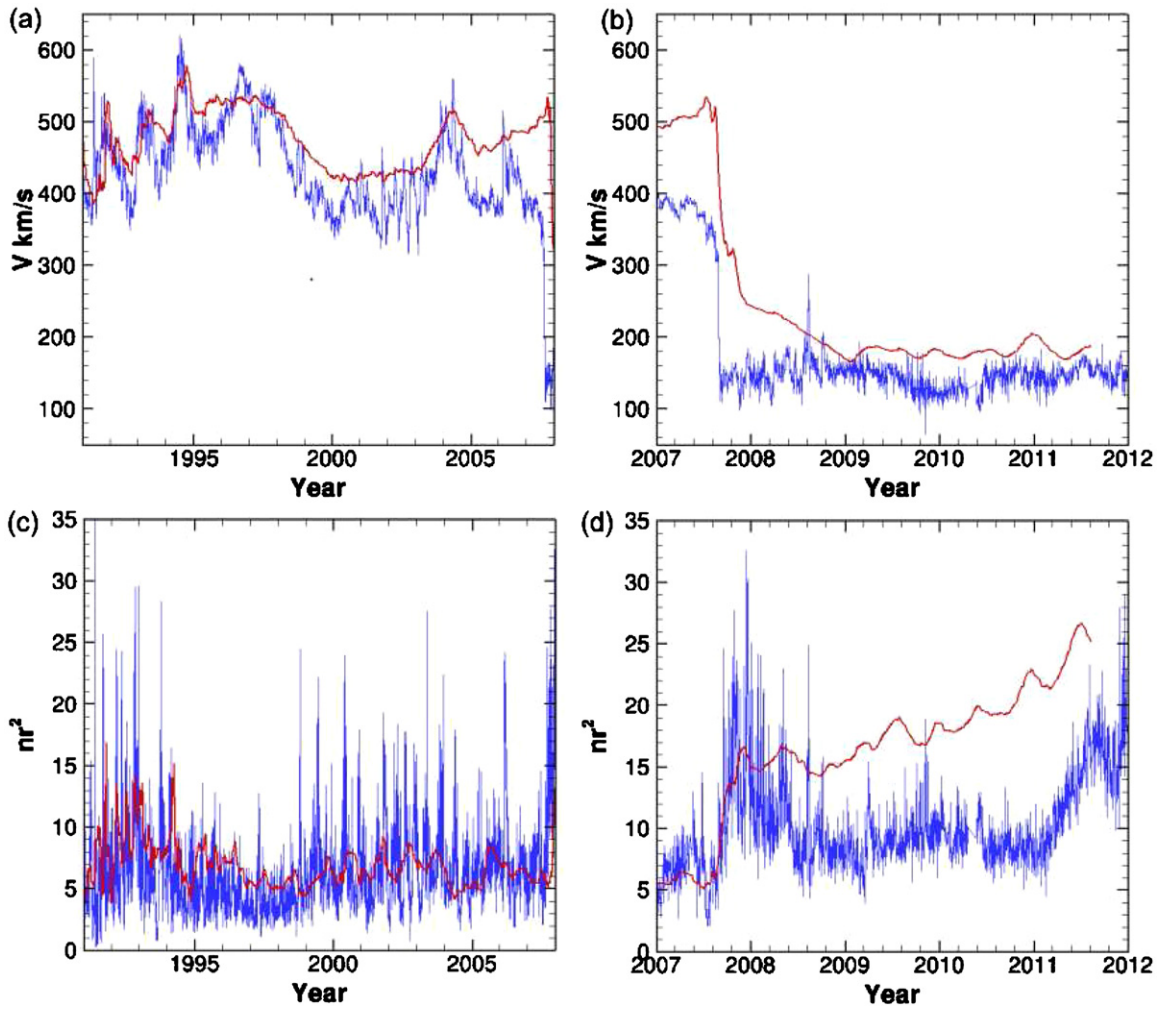

Figure 3. Comparison of the SW total speed and normalized number density nr^2 obtained in the three-dimensional time-dependent model along the *V2* trajectory with daily averaged *V2* observations: ((a) and (c)) supersonic SW; ((b) and (d)) heliosheath. For panels (b) and (d), model results were shifted in time by $\Delta t = 0.4$ yr to match the TS crossing by *V2*.

(A color version of this figure is available in the online journal.)

three-dimensional model. Since time-latitudinal variations of the heliospheric magnetic field (HMF) are unknown, we assume that HMF changes in time according due to the dependence of the azimuthal component of Parker's spiral magnetic field on the SW radial velocity (Parker 1958), which is a function of time in our boundary conditions.

Before running the three-dimensional time-dependent simulation, we obtain a three-dimensional steady state solution of the SW interaction with the LISM. In this case, for latitudinally dependent inner boundary conditions, we use values of the SW parameters obtained at 30 AU from one-dimensional steady state runs in each of the 19 latitudinal directions described above. Figure 2(a) shows the boundary conditions for the SW density and velocity which depend on latitude (but are constant in time). The latitudinal variations of the dynamic pressure shown in Figure 2(b) cause a blunter shape of the TS and HP than in the case of a spherically symmetric wind (Opher et al. 2009). This shape affects the plasma flow in the heliosheath and will be discussed in the next section. For the interstellar medium plasma we assumed: $V_{\rm LISM} = 26.4\,{\rm km\,s^{-1}}$, $n_{p_{\rm LISM}} = 0.06\,{\rm cm^{-3}}$, and $T_{\rm LISM} = 6519\,{\rm K}$. The number density of H atoms in the LISM is $n_{H_{\rm LISM}} = 0.18\,{\rm cm^{-3}}$. The interstellar magnetic field (ISMF) has a magnitude $B_{\rm LISM} = 4.4\,\mu{\rm G}$ and the orientation is specified by angles $\alpha = 20^\circ$ and $\beta = 60^\circ$. The models with this ISMF by Opher et al. (2009) and Izmodenov et al. (2009) showed a good agreement with the observed asymmetry of the TS. For the HMF we take a Parker spiral magnetic field with a radial component $B_{r,30} = 7.17 \times 10^{-3}$ nT at 30 AU at the equator. Also we assume that the Sun's magnetic and rotation axes are aligned.

Using the steady solution for the initial state, we performed a three-dimensional time-dependent simulation over 6 iterations (12 solar cycles) until the results of two subsequent iterations showed the same variations of the TS and HP. To capture the HP in the time-dependent simulations, we used a level-set method. At the steady state solution, we introduced the level-set function $f_{\rm HP}$ which is zero at the HP, positive inside the HP, and negative outside. To determine the location of the HP during the time-dependent simulation, we solve the equation $df_{\rm HP}/dt = 0$ which evolves the function $f_{\rm HP}$ with the plasma flow.

Our model has several limitations. It does not include effects of CIRs and the tilt of the solar magnetic axis relative to the solar rotation axis. Including these effects is computationally challenging (e.g., Opher et al. 2011 for tilt) and requires additional observational data for construction of SW boundary conditions (resolving CIRs and other transients in the SW).

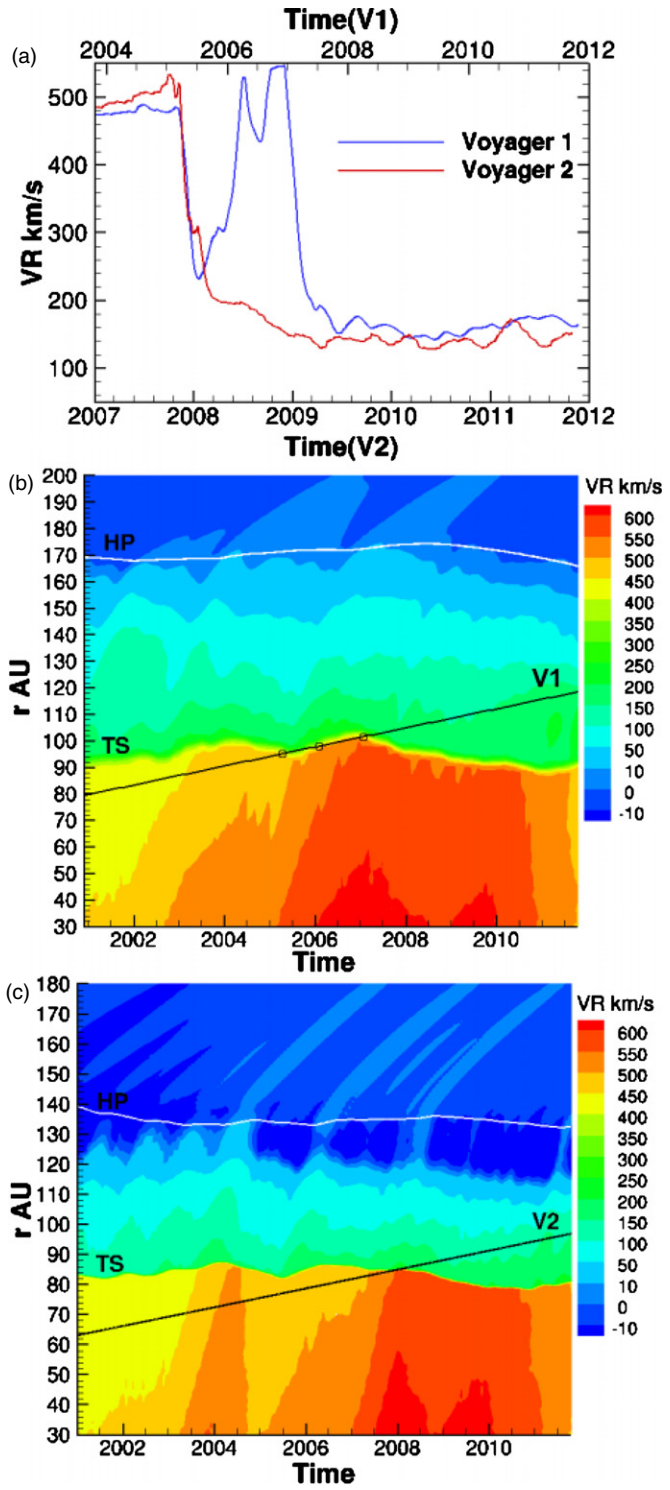

Figure 4. (a) Profiles of the plasma radial speed along the *V1* (blue curve) and *V2* (red curve) trajectories from a three-dimensional time-dependent model. Space–time distribution of the radial speed along the *V1* (b) and *V2* (c) trajectories. Circles denote TS model crossings by *V1*.

(A color version of this figure is available in the online journal.)

An alternative method of deriving the boundary conditions (latitude, longitude, and time-dependent) at 1 AU is from the SW models starting from the solar surface such as the Alfven-Wave-driven SOlar wind Model (AWSOM) which is part of the Space Weather Modeling Framework (SWMF; van der Holst et al. 2014) or the MHD Algorithm outside a Sphere (MAS)/ENLIL models (Odstrcil 2003). These models use magnetic field data at the boundary on the Sun obtained from synoptic magnetic maps available from different observations (*SOHO*/Helioseismic and Magnetic Imager, *SDO*/Michelson Doppler Imager, or Kitt Peak Observatory). Runs of these models can be requested on the NASA's Community Coordinated Modeling Center (CCMC) Web site. Propagating these solutions from 1 AU to the TS and HP is computationally demanding and, for the time that it takes the SW to reach the TS (∼year) and HP (∼4 yr), many CRs need to be included. Thus, it is not yet clear how feasible this approach would be.

3. RESULTS AND DISCUSSION

Figure 3 shows a comparison of the SW speed and normalized density nr^2 (where n is the plasma number density in cm^{-3} and r is the distance from the Sun in AU) calculated in the model along the *V2* trajectory with the observations. In a supersonic SW (Figures 3(a) and (c)), the model results are in good agreement with the measurements except for the period 1995–1999 for the density and 2005–2007 for the speed. A two-dimensional time-dependent kinetic-hydrodynamic model by Izmodenov et al. (2005) with latitudinally uniform boundary conditions at 1 AU taken from OMNI data (slow wind) showed that during the solar minimum in 1995–1999, the model did not reproduce the *V2* measurements. *V2* experienced a higher plasma speed than obtained in their model because the spacecraft was located in the fast wind. Our boundary conditions that take into account the fast SW allow us to get a good agreement between the model speeds and the data during the period 1995–1999 (Figure 3(a)). However, for the same period, the density is higher by a factor of ∼2 in the model as compared to the *V2* measurements (Figure 3(c)). Figure 3(a) shows that after 1999, the modeled speed exceeds *V2* observations by 50 km s^{-1} and the difference increases to 100 km s^{-1} as we approach the TS. This could be a result of insufficient slowdown of the SW due to charge exchange with interstellar hydrogen atoms (in our three-dimensional model the hydrogen density at the TS surface $n_{H,TS}$ is in the range 0.07 cm^{-3}–0.08 cm^{-3}). This hypothesis will be explored in future calculations using a higher hydrogen density in the LISM. Also, our model does not reproduce a strong increase of the SW speed associated with a shock detected at *V2* in 2006 March (Richardson et al. 2006) with a subsequent decrease closer to the TS crossing. The origin of this strong shock is the coronal mass ejection associated with the solar flare in 2005 September and polar fast streams (Richardson et al. 2006). Such local short timescale disturbances are not resolved in our SW data set at 1 AU since it is averaged over a solar rotation (or one year for IPS data). Therefore, they are not resolved in our simulation results. To reproduce this shock, data with a higher resolution in time (e.g., 1 hr averaged *Ulysses* data) need to be used as in Richardson et al. (2006).

Figures 3(b) and (d)) show the comparison for the heliosheath region. *V2* observations show that the plasma speed is nearly constant in the heliosheath with an average speed of 146 km s^{-1} (Richardson & Wang 2012). Our model shows that after crossing the TS, the plasma speed is about 240 km s^{-1} which is about 100 km s^{-1} higher than *V2* observed. By the end of 2008, the plasma speed decreases to a value of 180 km s^{-1} and then remains constant with an average speed of 185 km s^{-1}. Figure 3(d) shows that the modeled SW density is larger than the actual by a factor of two. After entering the heliosheath, *V2* experienced solar minimum conditions (at least until the beginning of 2011; Richardson & Wang 2012). The reason for

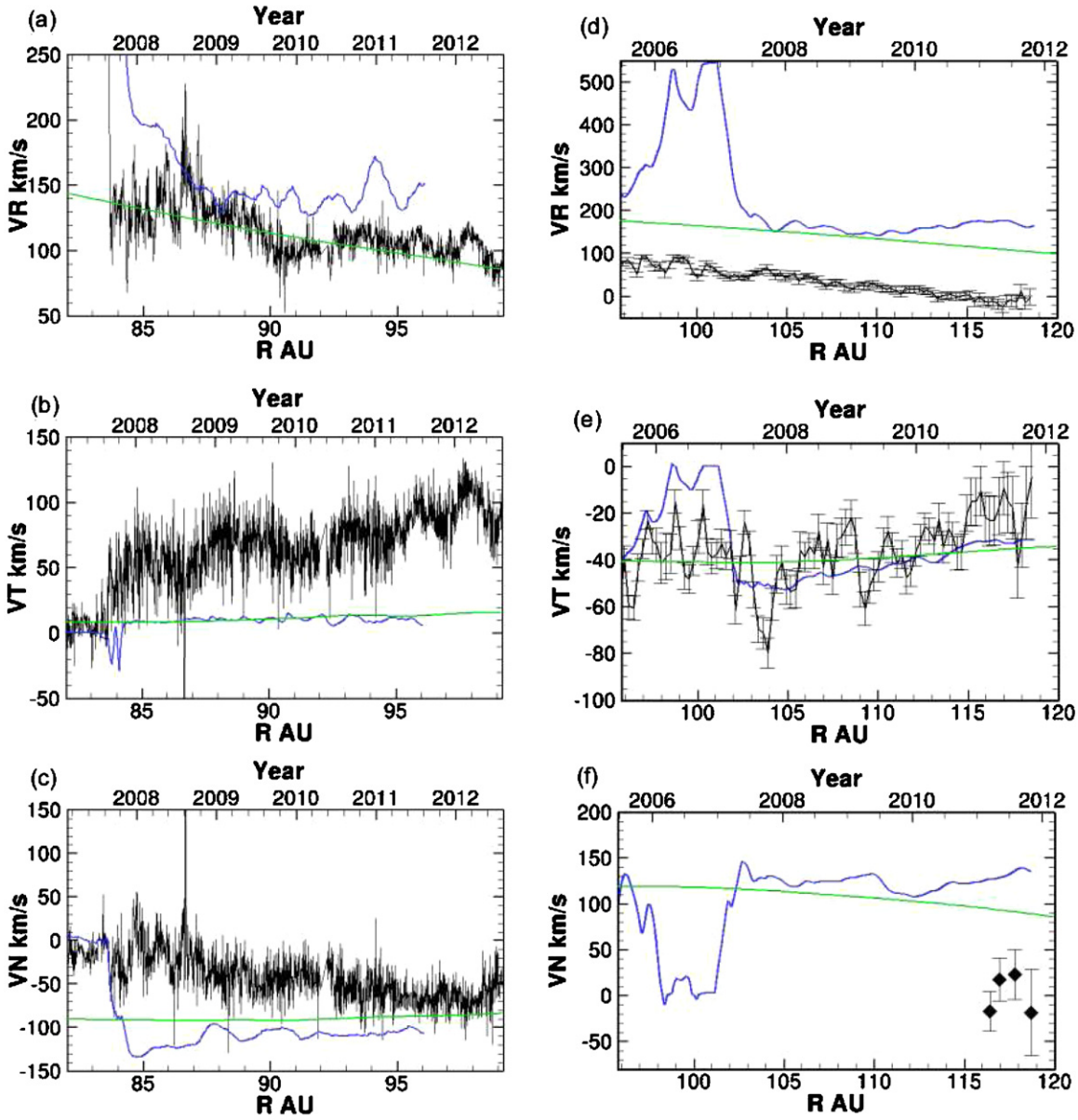

Figure 5. Components of the plasma velocity for *V2* (left column) and *V1* (right column). The black curve indicates daily averaged *V2* data ((a)–(c)) and 26 day averaged VR and VT components determined from LECP at *V1* ((d) and (e)). The black diamonds show measurements of VN from four rolls of *V1* during 2011 (f). Vertical error bars are Poisson statistical uncertainties on the mean. The blue curves show results of the time-dependent model and green curves are the results of the steady state solution. (VR, VT, and VN are radial, tangential, and meridional components of velocity, respectively.)

(A color version of this figure is available in the online journal.)

the difference in density between the model and observations during the solar minima both in the supersonic SW and in the heliosheath needs to be explored in a future study (as a first approach, the effect of the higher density in our boundary conditions than observed by *Ulysses* during the solar minimum should be investigated).

The time-dependent model predicts similar radial speeds in the heliosheath for *V1* and *V2* (Figure 4(a)). In the simulation, *V1*'s crossing of the TS occurred 0.3 yr later than observed because the distance to the TS in the model is slightly larger than what *V1* observed (by 3 AU). After *V1*'s crossing, the TS rapidly moves outward (Figure 4(b)) in response to the increase of the SW dynamic pressure from mid-2004 to the end of 2004 as seen in our data set at 1 AU. As a result, in the model, *V1* crossed the TS two more times as can be seen in Figures 4(a) and (b) (three crossings of the TS by *V1* are shown by circles). This did not actually occur with *V1*. We performed additional simulations in which the location of the TS was in agreement with the observed TS distance. In both cases, the modeled plasma radial speeds along the *V1* and *V2* trajectories are similar. Figures 4(b) and (c) show the time–space distribution of the radial speed for *V1* and *V2*. Figure 5 shows the VR, VT, and VN flow components (in the standard RTN coordinate system in which R is radially outward, T is a plane parallel to the solar equator and positive in the direction of solar rotation, and N completes a right-handed system) in the heliosheath calculated in the model along *V1* and *V2* trajectories. For comparison, we show *V2* observations and flows determined from LECP data on *V1*.

To determine the type of SW that *V2* observed in the heliosheath, we traced the flow at the *V2* location in time along the plasma streamline upstream of the TS. This procedure assumes that the streamlines are quasi-stationary. The model

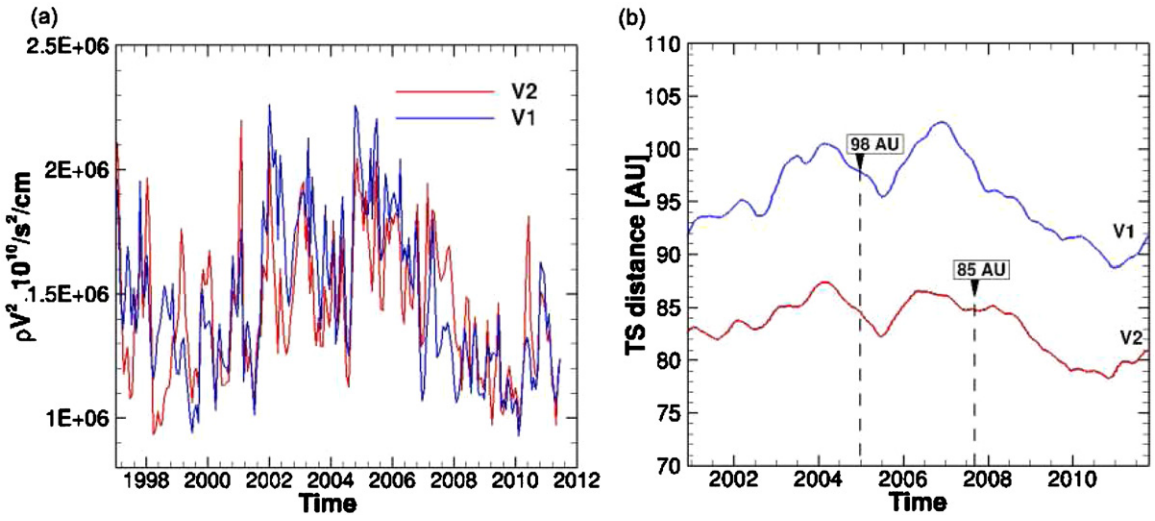

Figure 6. (a) Variations of the solar wind dynamic pressure at 1 AU at the heliolatitudes corresponding to *V1* and *V2* (approximately ±30°). (b) Variations of the distance to the TS in the directions of *V1* and *V2*.

(A color version of this figure is available in the online journal.)

shows that after the TS crossing, *V2* was immersed in a wind with original speeds of 500–550 km s^{-1} until 2009. Since then, *V2* has observed plasma flow with speeds upstream the TS of 450–500 km s^{-1}. *V2* observations show that after the end of 2009 the radial speed was constant with an average value 110 km s^{-1}. The steady-state solution yields VR decreasing by 30% (green curve in Figure 5(a)). The time-dependent model shows that the average VR is constant after the *V2* passes the distance 87 AU at the end of 2008. Qualitatively, this behavior of VR is consistent with the observations. However, the average value is about 140 km s^{-1}, which is higher than observed.

The model results show that *V1* recrossed the TS and moved into the supersonic SW in 2005 so at this point, the speed increased and the density decreased (Figure 4(b)). After 2007, the time-dependent model predicts essentially a constant VR for *V1* with an average value of 160 km s^{-1}. Therefore, the model predicts similar behavior of the radial flows along *V1* and *V2*. However, the flow speeds in the heliosheath derived from *V1* LECP data are slower than the actual for *V2* and decreased across the heliosheath from ∼70 km s^{-1} to ∼0 km s^{-1} at 113 AU (Krimigis et al. 2011). We conclude that while the solar cycle effects can reproduce the constant radial speed in the heliosheath at *V2* (at least after 2009), they do not reproduce the decrease of VR to zero seen for *V1*.

Modeled values of VN at *V1* and *V2* are much higher than in the observations. The average VN at *V2* in the model is −110 km s^{-1} while the observations indicate −50 km s^{-1}. In the model, the average VN at *V1* is 130 km s^{-1}. During re-orientations of *V1* in 2011–2012, observations show VN is near zero (Decker et al. 2012). Also, VN components in our model are different from those obtained in the steady state model with spherically symmetric SW (V_{sw} = 400 km s^{-1}, n_{sw} = 0.00874 cm^{-3}). Results of Alouani-Bibi et al. (2011) showed VN ≈ 50 km s^{-1} at *V1* and VN ≈ −40 km s^{-1} at *V2*. High values of VN in our time-dependent model are caused by the strong bluntness of the TS and HP in the N direction.

Besides the bluntness of the heliosphere, the tangential flows (VT) are very sensitive to the geometry of the heliopause as affected by the orientation of the ISMF (B_{ISM}). As the orientation of B_{ISM} changes, VT changes dramatically (for a change of 30° in the plane of B_{ISM} VT changes ∼20 km s^{-1}; for a change in 60°, VT changes by 30 km s^{-1}; Opher et al. 2012). In our model, VT for *V2* is about 10 km s^{-1} with an increase with distance by 50% (Figure 5(b)) which is much smaller than the VT observed (about 50 km s^{-1} with gradual increase to 100 km s^{-1}). The VN and VT presented in Figure 5 indicate that the TS and HP are blunter in the N than in the T directions and the heliosheath is higher than wider. Based on the *V2* data, Richardson et al. (2009) reported the opposite structure, namely, that the TS is blunter in the T direction than in the N direction. The inconsistency is caused by the shape of the heliospheric boundaries in our solution determined by the average latitudinal variations of the SW dynamic pressure which has two maxima at the middle latitudes as shown in Figure 2(b). Our results show that the solar cycle effects do not bring the modeled shape of the heliosphere into agreement with the actual for *V2*.

Figure 6(b) shows variations of the distance to the TS with time in response to the changing SW dynamic pressure at 1 AU in the model (Figure 6(a)). Maximum and minimum distances to the TS occur about a year after the corresponding maximum and minimum of the SW dynamic pressure at 1 AU. The minimum distances to the TS are 78 AU in the *V2* direction (in 2010.8) and 88 AU in the *V1* direction (in 2011). After 2011, the TS distance increases due to the recovery of the dynamic pressure. In the model, the distance to the TS is slightly larger than what *V1* and *V2* observed. Dashed lines in Figure 5 denote the times when spacecraft crossed the TS. The model produces 13 AU of asymmetry in the TS distances which is slightly higher than 10 AU asymmetry observed by the *Voyager* spacecraft.

Figure 7 shows variations of the distance to the HP in the direction of *V1* (blue curve with corresponding left axis) and *V2* (red curve with corresponding right axis). The HP reflects changes in the SW dynamic pressure at 1 AU with approximately a four year lag. Outward motion of the HP is caused by the increasing SW dynamic pressure starting around 1999 (Figure 6(a)). The decreasing SW dynamic pressure since 2005–2006 caused the HP to move inward starting around 2009. The model predicts that the minimum distance to the HP due to the low SW dynamic pressure in 2008–2009 would be expected in 2013. However, since overall variations of the HP distance during the solar cycle are less than 10 AU, this minimum

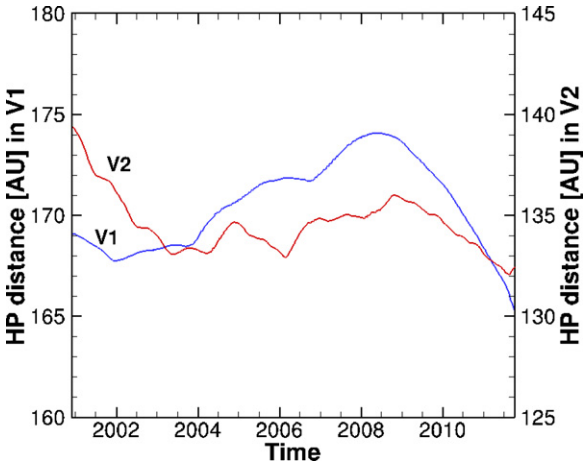

Figure 7. Variations of the distance to the HP in the directions of *V1* (blue curve with corresponding left *Y*-axis ranging from 160 to 180 AU) and *V2* (red curve with corresponding right *Y*-axis ranging from 125 to 145 AU) trajectories. (Small-scale variations are resolved better in the *V2* than in *V1* direction because of higher resolution of the grid in the V2 direction.)

(A color version of this figure is available in the online journal.)

distance is still larger than the distance at which *V1* crossed the heliopause, ∼121 AU (Gurnett et al. 2013).

4. CONCLUSIONS

In this paper, we presented results of a study of the effects of solar cycle on the SW flows in the heliosheath. We improved a three-dimensional MHD model of the interaction of the SW with the local interstellar medium by implementing time and latitudinally dependent boundary conditions for the SW derived from *SOHO*/SWAN backscattered solar Lyα emission data and radio observations from IPS. These observational data provide latitudinal SW variations during two full solar cycles. In our analysis of model results of the SW flows in the heliosheath, we focused on two directions, the trajectories of the *V1* and *V2* spacecraft, and compared the model results with *Voyager* data. The time-dependent model predicts different radial speed in the heliosheath along the *V2* trajectory than a steady state model. After an initial period of perturbed plasma (until 2009) the model predicts constant average radial speed at *V2*. Within 30 AU from the TS, *V2* was immersed in the SW, which varies by 50 km s^{-1} in speed upstream of the TS and which is faster than the slow wind by 100 km s^{-1}, accounting for the lack of a decrease in speed with radii expected from steady state models. The meridional velocity component VN is much larger and the VT is much smaller in the model than in the *V2* observations. In our model, the TS and HP are blunter in the N than in the T direction, which is not consistent with *V2* data that suggest the opposite shape. This discrepancy in the shape of the TS and HP can be related to the $B_{\rm LISM}$ and/or latitudinal variation of the SW dynamic pressure defined by the SW boundary conditions at 1 AU in our solution.

Additionally, we found that the modeled plasma density along the *V2* trajectory is higher than the *V2* observations by a factor of two during the solar minimum in both the supersonic SW (1995–1999) and in the heliosheath (2008–2012). The reason for this difference in density between the model and observations needs to be investigated in a future study (as a first approach, the effect of a higher density in our boundary conditions as compared to *Ulysses* data during the solar minimum will be explored). However, the disagreement between the density predicted by the model and the observations lasted for years while the SW data set used in our simulations disagrees with *Ulysses* (mostly in the SW density) only during short periods of time (∼1 yr).

The time-dependent model predicts a constant radial speed around 160 km s^{-1} in the heliosheath for *V1* while the indirect observations show a decrease in VR from 70 km s^{-1} to zero not seen in our model. The solar cycle model produces similar radial flow speeds at *V1* and *V2* in the heliosheath which does not agree with the observations. In our model for SW boundary conditions, we used time and latitudinal variations of the SW density and velocity obtained from SWAN/*SOHO* Lyα intensity maps and IPS measurements. Other solar cycle models of the outer heliosphere that incorporate idealized solar cycle (Pogorelov et al. 2009) or latitudinal profiles of SW parameters created from *Ulysses* data (Pogorelov et al. 2013) also showed that simulated flows in the heliosheath do not agree with *Voyager* data: the models (with certain assumptions) can reproduce radial velocities at *V1* and *V2* but modeled VT and VN flow components do not agree with observations. We do not expect that the difference in the SW dynamic pressure between the SW data used in this work and that observed by *Ulysses* has much effect on our results since these differences last only short periods of time (∼ year). The differences found between the model results and *Voyager* data have been observed over years. This indicates the potential importance of other physical processes (e.g., reconnection, turbulence, instabilities) in the plasma flows in the heliosheath that are not included in this model. Additionally, the boundary conditions for the SW in the models should be improved in the future. As shown above, while the overall agreement between the SW data set used in our model and *Ulysses* data is fairly good, there are some local differences. One possible approach for producing SW boundary conditions at 1 AU is using SW models starting from the solar surface such as those available at the NASA CCMC. However, this approach is extremely computationally challenging.

This research benefited from discussions at the meetings of the Heliopause Team at the ISSI in Bern, Switzerland. We thank O. Katushkina for providing us with the SW data set at 1 AU and for useful discussions. These data are based on *SOHO*/SWAN, OMNI database, and IPS results. IPS data analysis was performed by J. Sokol and M. Bzowski. Analysis of the *SOHO*/SWAN maps was carried out by the *SOHO*/SWAN team. We thank Robert Decker for providing us with the data on plasma flows derived from LECP/*Voyager 1* measurements for comparison with our model results. This work was supported by NSF CAREER Grant ATM-0747654. The calculations were performed with the NASA AMES Pleiades Supercomputer. V.I. and E.P. acknowledge partial support by RFBR grant 14-02-00746. J.D.R. was supported by the NASA *Voyager* project through JPL. M.O. was supported by NASA grant NNX13AE04G.

REFERENCES

Alouani-Bibi, F., Opher, M., Alexashov, D., Izmodenov, V., & Toth, G. 2011, ApJ, 734, 45
Baranov, V. B., & Zaitsev, N. A. 1998, GeoRL, 25, 4051
Decker, R. B., Krimigis, S. M., Roelof, E. C., et al. 2005, Sci, 309, 2020
Decker, R. B., Krimigis, S. M., Roelef, E. C., & Hill, M. E. 2012, Natur, 489, 124
Gurnett, D. A., Kurth, W. S., Burlaga, L. F., & Ness, N. F. 2013, Sci, 341, 1489
Izmodenov, V., Malama, Y. G., & Ruderman, M. S. 2005, A&A, 429, 1069
Izmodenov, V., Malama, Y. G., & Ruderman, M. S. 2008, AdSpR, 41, 318

Izmodenov, V. V., Malama, Y. G., Ruderman, M. S., et al. 2009, SSRv, 146, 329
Karmesin, S. R., Liewer, P. C., & Brackbill, J. U. 1995, GeoRL, 22, 1153
Katushkina, O. A., Izmodenov, V. V., Quemerais, E., & Sokol, J. M. 2013, JGR, 118, 2800
Krimigis, S. M., Roelof, E. C., Decker, R. B., & Hill, M. E. 2011, Natur, 474, 359
Kubiak, M. A., Bzowski, M., Sokol, J. M., et al. 2014, ApJS, 213, 29
Lallement, R., Quemerais, E., Lamy, P., et al. 2010, in ASP Conf. Ser., Vol. 428, SOHO-23: Understanding a Pecular Solar Minimum, ed. S. R. Cranmer, J. T. Hoeksema, & J. L. Kohl (San Francisco, CA: ASP), 428
Odstrcil, D. 2003, AdSpR, 32, 497
Opher, M., Bibi, F. A., Toth, G., et al. 2009, Natur, 462, 1036
Opher, M., Drake, J. F., Swisdak, M., et al. 2011, ApJ, 734, 71
Opher, M., Drake, J. F., Velli, M., Decker, R. B., & Toth, G. 2012, ApJ, 751, 80
Parker, E. 1958, ApJ, 128, 664
Pogorelov, N. V., Borovikov, S. N., Zank, G. P., et al. 2012, ApJL, 750, L4
Pogorelov, N. V., Borovikov, S. N., Zank, G. P., & Ogino, T. 2009, ApJ, 696, 1478
Pogorelov, N. V., Suess, S. T., Borovikov, S. N., et al. 2013, ApJ, 772, 2
Provornikova, E., Opher, M., Izmodenov, V., & Toth, G. 2013, A&A, 552, A99
Quemerais, E., Lallement, R., Ferron, S., et al. 2006, JGR, 111, A09114
Richardson, J. D., Liu, Y., Wang, C., et al. 2006, GRL, 33, L23107
Richardson, J. D., Stone, E. C., Kasper, J. C., Belcher, J. W., & Decker, R. B. 2009, GRL, 36, L10102
Richardson, J. D., & Wang, C. 2012, ApJL, 759, L19
Scherer, K., & Fahr, H. J. 2003, GeoRL, 30, 1045
Sokol, J. M., Bzowski, M., Tokumaru, M., Fujiki, K., & McComas, D. J. 2012, SoPh, 285, 167
Tokumaru, M., Kojima, M., & Fujiki, K. 2012, JGR, 117, A06108
Toth, G., van der Holst, B., Sokolov, I. V., et al. 2012, JCoPh, 231, 870
van der Holst, B., Sokolov, I. V., Meng, X., et al. 2014, ApJ, 782, 81
Wang, C., & Belcher, J. W. 1999, JGR, 104, 549
Washimi, H., Zank, G. P., Hu, Q., et al. 2011, MNRAS, 416, 1475
Zank, G. P. 1999, in AIP Conf. Proc. Vol. 471, Solar Wind 9, ed. S. Habbal, R. Esser, J. Hollweg, & P. Isenberg (Melville, NY: AIP), 783
Zank, G. P., & Muller, H.-R. 2003, JGR, 108, 1240
Zubkov, V. 2005, in Proc. Solar Wind 11/SOHO 16, ed. B. Fleck, T. H. Zurbuchen, & H. Lacoste (ESA SP-592; Noordwijk: ESA), 164